Published in final edited form as:

Nat Methods. 2011 February ; 8(2): 171–176. doi:10.1038/nmeth.1548.

A microfluidic array for large-scale ordering and orientation of embryos

Kwanghun Chung[#1], **Yoosik Kim**[#2], **Jitendra S. Kanodia**[2], **Emily Gong**[1], **Stanislav Y. Shvartsman**[2], and **Hang Lu**[1,*]

[1]School of Chemical & Biomolecular Engineering and Parker H. Petit Institute for Bioengineering & Bioscience, Georgia Institute of Technology, Atlanta, GA 30332-0100, USA

[2]Department of Chemical and Biological Engineering and Lewis-Sigler Institute for Integrative Genomics, Princeton University, Princeton, NJ 08544, USA

[#] These authors contributed equally to this work.

Abstract

Quantitative studies of embryogenesis require the ability to monitor pattern formation and morphogenesis in large numbers of embryos, at multiple time points, and in diverse genetic backgrounds. We describe a simple approach that greatly facilitates these tasks for *Drosophila melanogaster* embryos, one of the most advanced models of developmental genetics. Based on passive hydrodynamics, we developed a microfluidic embryo trap array that rapidly orders and vertically orients hundreds of embryos. We describe the physical principles of the design and use this platform for the quantitative analysis of multiple morphogen gradients in the dorsoventral patterning system. Our approach can also be used for live imaging, and, with slight modifications, could be adapted for studies of pattern formation and morphogenesis in other model organisms.

Keywords

microfluidics; imaging; Drosophila; high-throughput; quantitative analysis; morphogen gradient; dorsoventral pattern formation; systems biology

INTRODUCTION

Spatial control of cell differentiation in embryos can be provided by the graded distribution of morphogens, chemical signals that act as dose-dependent regulators of gene expression. Some of the first morphogen gradients were identified in the *Drosophila* embryo, where the dorsoventral (DV) axis of the embryo is patterned by the nuclear localization gradient of

[*]Correspondence should be addressed to HL, hang.lu@gatech.edu, 1-404-894-8473 (ph), 1-404-894-4200 (fax).

AUTHOR CONTRIBUTIONS

KC, EG, and HL designed, fabricated, and tested the device. YK tested the device and performed imaging. JSK wrote the image processing and statistical programs for gradient quantification. KC, YK, SYS and HL designed the experiments and wrote the paper.

COMPETING FINANCIAL INTEREST

The authors declare no competing financial interests.

Dorsal (Dl), an NF-κB transcription factor, which subdivides the embryo into three germ layers[1-3] (**Fig. 1a,b**). The regions exposed to high, medium, and low levels of Dl, respectively, contribute to the formation of the mesoderm, the nervous system, and the skin of the embryo.

Quantitative analysis of developmental systems controlled by morphogens requires information about both the regulatory regions of genes comprising the network and the spatial distribution of patterning signals. The DV patterning system in *Drosophila* is arguably one of the best understood systems with regard to its sequence-specific transcriptional regulation. However, information about the distribution of patterning signals is currently lacking, mainly due to technical difficulties associated with imaging the spatial distribution of proteins and transcripts along the DV axis of the embryo[4,5]. When imaged on a regular microscope slide, embryos are oriented with their major axis parallel to the cover slip, and their DV orientation is essentially random. Since only a small fraction of embryos can be used for quantitative imaging, previous analyses of signals in the DV system relied on data collected from ~10 embryos[6,7].

To enable high-throughput analysis of the DV patterning signals, we developed a microfluidic embryo trap array, a device in which hundreds of embryos are oriented vertically in a matter of a few minutes. Such “end-on” orientation allows for DV axis data to be easily collected from multiple embryos. Previously, end-on imaging has been possible only for very small numbers of embryos, which had to be individually and manually placed into an upright position[5,6].

In this paper, we describe the design and the physical principles of the embryo trap array and demonstrate how it can be used in to quantify morphogen gradients in fixed embryos and to monitor nuclear divisions in live embryos. The device enables high-throughput analysis of the dorsoventral patterning system at the level of the inductive cues and their signaling and transcriptional targets in multiple genetic backgrounds. Using this device to image a large number of embryos, we resolve an outstanding issue regarding the spatial extent of the Dl morphogen gradient.

RESULTS

Design of the embryo trap array

The array is a one-layer microfluidic device fabricated from polydimethylsiloxane (PDMS), an optically transparent elastomer widely used in biological microfluidics[8,9]. In order to allow for imaging of a large number of embryos, the array needs to have traps that are densely packed, which is an engineering challenge. Conventional approaches using hydrodynamics for cell trapping typically do not achieve such high packing density[10,11], mostly due to the requirement to properly balance flow resistance, resulting in a relatively large space between neighboring traps. The mechanism used in our design, in contrast, does not rely on resistance change upon the occupation of traps, and therefore allows for densely arraying ~700 traps in the space of a microscope slide (**Fig. 1c, d**).

Our design consists of a serpentine fluid-delivery manifold and an array of cross-flow channels (**Fig. 1c, d**). The 700-μm wide serpentine channel is wider than the major axis of the embryo (~500 μm) allowing embryos of any orientation to move easily through it. This feature is particularly important for robust handling of non-spherical objects like *Drosophila* embryos. Each cross-flow channel includes a truncated cylindrical trap where the embryo is located for imaging; the trap is connected to a narrowing channel and a long and narrow resistance channel (**Fig. 1d, e**). When an embryo approaches an empty trap, the flow through the trap will guide it into the trap (**Fig. 1f**). The shape of the trap dictates that the embryo is in an upright position for imaging (**Fig. 1g**) such that each embryo on every device is oriented with the dorsal-ventral plane horizontal. Oriented embryos, which appear round when viewed from the top, are thus arrayed on the device (**Fig. 1h**).

Using a computational fluid dynamics approach (**Online Methods**), we engineered the hydrodynamic resistances of the cross-flow channels. A simplified smaller array in a three-dimensional computational model (**Supplementary Fig. 1**) demonstrates that our design satisfies the following criteria. First, all the traps are exposed to similar flow rates (**Fig. 2a**). If the flow in the array has large variations in different rows or columns, the trap occupancy would be severely compromised; optimal design, however, yields highly repeatable near-perfect occupancy, as we show experimentally (**Supplementary Fig. 2**). Second, the bulk of the embryo suspension flows along the serpentine manifold (compare flow rates of **Fig. 2a, b**). The bulk flow through the main channel efficiently sweeps out extra and improperly trapped embryos (**Supplementary Video 1**). In addition, too low a cross flow through the traps prevents embryos from being introduced to the traps, resulting in inefficient trapping (blue region in **Fig. 2b**); on the other hand, too high cross flow causes embryos to accumulate near traps and clump together (yellow region in **Fig. 2b**). Thus, optimal design of an array that works well with *Drosophila* embryos required proper parameter choice, including geometry and operating pressure range.

Another important mechanism for orientation of embryos in our device is the presence of a significant Dean flow (with a Dean number greater than 100 throughout the device), an effect in which curvature of the channel induces a secondary non-axial flow[12]. This hydrodynamic effect is apparent in the stream-line trace in **Fig. 2c** and in frames from an embryo loading video (**Fig. 2d**). The Dean flow and the diverging and converging flow through the cross-flow channels focus the embryos towards the traps (as opposed to embryos distributing in random locations in the bulk flow), and significantly increases the frequency with which embryos contact the traps and are loaded into them. The presence of the secondary Dean flow at the bends of the channel not only greatly improves trap occupancy, but also maximizes loading efficiency since an embryo has many opportunities to be in contact with an empty trap. In fact, essentially every single embryo entering the device is trapped, a feature that will be very useful in studies where one has to work with small numbers of embryos in complex genetic backgrounds. Experimentally we observe that the percent of traps loaded with embryos is ~90%.

During the loading process, the entire device is under a slight positive pressure. Because the PDMS is an elastomer, the pressure can expand the trap opening[13] to facilitate loading (**Fig. 1f** and **Fig. 2e-j).** Confocal microscopy characterization of trap behavior under different

pressures (**Fig. 2e, h**) demonstrates that at ambient condition (0 psi), the traps have smaller openings (not enough for an embryo to be loaded or released), as compared to under 6 psi of positive pressure. When operating the device, we first connect the device at the outlet to a pressure-drop tube to raise the average pressure of the device to ~6 psi to open the traps. The embryo suspension is then introduced into the device using a syringe or a pressure source (e.g. compressed air).

Under flow conditions, embryos at the traps experience non-uniform pressure and shear by the surrounding fluid; the resulting force flips the embryo vertically, inserting it into the cylindrical trap (**Fig. 1f** and **Supplementary Fig. 3**). This is achieved entirely passively by hydrodynamics, without user intervention or control. Once the loading process is completed, the injection pressure is reduced, and the trap opening contracts, securing the embryo inside in an up-right position (with DV axis parallel to the cover slip, **Fig. 1f**, **Fig. 1e**, and **Supplementary Video 2**). This lock-in feature allows the device to be disconnected from the rest of the hardware, transported for imaging, or stored with the embryos embedded. Because the operation of the device consists of two simple steps and does not require a computer, valves, or other off-chip components except a pressure source, it can be easily used by non-experts easily. Because the embryos have different sizes and shapes and because antibody staining can be highly variable, typically large numbers of embryos are needed. We quantified DAPI staining in many embryos in the trap array showing that the variability of the supposedly uniform signal along the DV axis is negligible compared to the gradients that we typically quantify (**Supplementary Fig. 4**) Thus, the device also does not introduce illumination bias in the embryos.

Quantitative imaging of pattern formation

We used the embryo array to analyze the distribution of the nuclear levels of Dorsal (Dl), a transcription factor that initiates dorsal-to-ventral (DV) patterning of the *Drosophila* embryo. The ventral-to-dorsal distribution of nuclear Dl is induced by localized activation of the Toll receptor on the ventral side of the embryo[14]. Prior to Toll activation, Dl is sequestered in the cytoplasm, in a complex with its binding partner Cactus[15]. In response to Toll signaling, Cactus is degraded and Dl moves into the nucleus, where it binds the regulatory regions of its target genes.

One of the outstanding questions in DV patterning is the spatial extent of the Dl gradient[16]. More specifically, it is not clear over what part of the DV axis the Dl gradient is flat, and where it therefore cannot act as a patterning signal. This has been a matter of intense debate in recent publications[6,7,16,17]. The disagreements in the literature may be traced to current methodological limitations in quantification of the Dl gradient. While end-on imaging provides information about the entire DV axis, it has only been possible to apply it to a few embryos until now[5,6,18]. Lateral imaging, on the other hand, can be applied to more embryos and to imaging a larger number of gradients, but it is limited to only a fraction of the DV axis[7,17]. Our platform substantially increases the statistical power of end-on imaging, allowing us to investigate the spatial extent of the Dl gradient.

The lowest level of nuclear Dl is at the dorsal-most point of the embryo, which corresponds to the lowest level of Toll activation. If the level of nuclear Dl at an arbitrary position *x*

along the DV axis is statistically indistinguishable from the nuclear Dl level at the dorsal side of the embryo, then the Dl gradient can be considered flat between the position *x* and the dorsal-most position. We compared the distribution of nuclear Dl along the DV axis to the nuclear Dl levels at the dorsal-most point of the embryo. We conducted over 10 independent experiments, each collecting Dl gradients from at least 50 embryos during the last nuclear division cycle before cellularization 70 μm from the poles (**Fig. 3a-e**). For each of these datasets, we used a pair-wise statistical test to find the DV position at which the mean of the nuclear Dl level becomes indistinguishable from the value at the dorsal side of the embryo; differences were considered significant for $P < 0.01$.

Based on this analysis, we can estimate the spatial range of the Dl gradient reaches to ~60% of the DV axis. Thus, any gene expression boundary located outside of this range cannot be explained by a model based on the direct control by the Dl gradient. As an example, we consider the regulation of *zerknüllt (zen)*, a transcription factor expressed on the dorsal side of the embryo[19]. This gene is expressed in a dynamic pattern that first covers the dorsal half of the embryo (**Fig. 3f-h**). The expression boundary is well within the estimated range of the Dl gradient, consistent with previous studies suggesting that Dl represses zen [19]. At a later time point, the *zen* expression boundary moves to ~ 90% of the DV axis (**Fig. 3f,g**), outside of the estimated range of the Dl gradient, which suggests a more complex mode of regulation. Indeed, previous studies revealed that the later phase of *zen* expression depends on Dl only indirectly (**Fig. 3h**)[20].

Quantitative analysis of DV patterning requires systematic analysis of multiple transcriptional and signaling targets of Dl, in both the wild type and mutant backgrounds. The embryo array can be readily used to statistically compare spatial patterns across multiple genetic backgrounds[21]. For instance, Dl gradients in wild-type embryos and embryos derived from mothers with only a single copy of the *dl* gene (**Fig. 3i-k**) show that the nuclear Dl levels in the latter are reduced throughout the DV axis. Note that the nuclear Dl levels are reduced to only 80% of their wild-type value (**Fig. 3k**).

We analyzed the distribution of other regulators of DV patterning. This system is dominated by feedforward loops, a network motif in which a gene is controlled both by the primary input, such as Dl, and by one of its more proximal targets (**Fig. 4a**)[22]. For instance, Snail (Sna), a transcription factor expressed in the future mesoderm, is activated both by Dl and by Twist (Twi), a transcription factor that is directly activated by Dl. Patterning of the neurogenic ectoderm requires a two-peaked pattern of signaling through the Mitogen Activated Protein Kinase (MAPK) cascade. This in turn reflects localized expression of components of the Epidermal Growth Factor Receptor pathway, which are activated by Dl and Twi and repressed by Sna. Finally, the dorsal ectoderm is patterned by the gradient of signaling through the Bone Morphogenetic Protein (BMP) pathway, which is spatially regulated by Dl and its multiple targets.

We used the embryo array to characterize Twi expression gradients, as well as gradients of MAPK and BMP signaling (**Fig. 4b-g**). Twi and BMP signaling gradients are consistent with the ones reported elsewhere[6,7,17,23], but the MAPK phosphorylation gradient (dpERK) is quantified here for the first time. We observed a significant level of MAPK activation at

the ventral-most region of the embryo (**Fig. 4g**). Furthermore, we found that Cic, a transcriptional repressor that is degraded as a consequence of its phosphorylation by MAPK[24], is significantly downregulated at the ventral side of the embryo (data not shown), supporting the notion that the ventrally activated MAPK contributes to DV patterning.

DISCUSSION

We have designed and tested a microfluidic platform for high-throughput end-on imaging of *Drosophila* embryos. This approach dramatically increases the efficiency of collecting and analyzing the signaling and transcriptional patterns along the DV embryonic axis. Until now, end-on imaging was not ideally suited for quantitative and statistical studies of pattern formation[5,6,18]. Using our microfluidic embryo trap array, hundreds of embryos can be oriented in an upright position in a matter of minutes. We have shown that datasets from dozens of embryos are sufficient for statistical analysis of spatial patterns in both the wild type and mutant backgrounds. Embryo array-based imaging has provided quantitative characterization of the Dl gradient and identified new features of DV patterning.

In the future, the temporal resolution of end-on imaging can be increased by grouping the images collected from fixed samples into distinct temporal classes. This could be based on cytological markers, such as the nuclear density in the syncytium or the extent of membrane invagination during cellularization. Furthermore, in preliminary experiments we established that live embryos can be successfully loaded into and imaged in the device as well. We obtained videos of cell divisions in the early embryo as well as in an embryo undergoing gastrulation (**Fig. 5** and **Supplementary Videos 3 and 4**); these embryos in the embryo trap array can go on and hatch normally.

Unlike the anterioposteior (AP) patterning system, which has been a subject of extensive mathematical modeling and computational analysis[25,26], comprehensive quantitative models of the DV system have yet to be developed[27,28]. This is now a feasible goal, enabled by the efficiency of end-on imaging in our platform. Furthermore, embryo-array based imaging is not limited to the analysis of pattern formation in the early embryo. Other related developmental events, such as gastrulation, could be readily analyzed using this system. Devices for related fly species can be readily designed by modifying the trap size for embryos that are smaller or larger than those of *D. melanogaster*. Finally, because we have shown a general method for handling non-spherical objects, which is significantly more difficult than handling cells, we expect that similar microfluidic designs can be used to image pattern formation and morphogenesis in other model organisms of developmental genetics.

ON-LINE METHODS

Microfluidic device fabrication

A mold was first fabricated by photolithographic processes. In the first step, a negative photoresist (SU8-2100, Microchem) was spin-coated twice at 400-600 rpm onto a silicon wafer to form a ~500 μm-thick layer. Features on a transparency mask were transferred to the SU-8 coated wafer by standard UV photolithography. The mold was then treated with

tridecafluoro-1,1,2,2-tetrahydrooctyl-1-trichlorosilane vapor (United Chemical Technologies) in a vacuum desiccator to prevent adhesion of PDMS during the molding process.

For fabricating the PDMS devices, a mixture of PDMS (parts A and B in 15:1 ratio) was poured onto the mold to give a ~1 mm-thick layer and partially cured at 70 °C for 20 min. A mixture of PDMS (part A and B in 10:1 ratio) was then poured on top to form ~ 4 mm-thick layer and cured at 70 °C for two hours. After peeling off the 5-mm PDMS layer, the individual devices were cut out, and access holes were punched in the PDMS. The devices were then treated with oxygen plasma and bonded to a cover glass.

Microfluidic device operation

Drosophila embryos were suspended in 100 mL PBS buffer in a glass bottle which was connected to the inlet of the device. The outlet of the device was connected to a long PE90 tubing. The high resistance of the long PE90 tubing makes the pressure drop along the device less than 20 % of the total pressure drop. This allows the traps to expand uniformly throughout the device. To load the embryo suspension into the device, a constant pressure source (~6 psig) was applied to drive the flow into the device. Precise pressure is not critical. After loading, the injection pressure was slowly decreased to 0 psig. All tubing was then disconnected from the device for imaging and storage.

Confocal microscopy was performed on a Zeiss LSM 510 VIS Confocal Microscope. The device was filled with fluorescent dextran (70,000 MW, Oregon Green, Invitrogen) solution. The pressure (0 psig to 6 psig) was controlled using a portable air compressor. Note that during normal operation of the device, a thumb-driven syringe to approximate this pressure range or a tank of compressed gas would also serve the same purpose.

Fly strain and whole-mount immunostaining

OreR flies were used as a wild type strain and dl^6 flies were used as *dl* heterozygous mutant strain in this study. Flies were raised and embryos were collected at 25 °C. Antibody staining was performed as described previously[21]. The following primary antibodies were used: rabbit anti-dpERK (1:100, Cell Signaling), mouse anti-Dorsal (1:100, Developmental Hybridoma Bank), guinea pig anti-Twist (1:40, a gift from M. Levine), and rabbit anti-phospho-SMAD (1:3500, a gift from D. Vasiliauskas, S. Morton, T. Jessell and E. Laufer, Columbian University). DAPI (1:10,000, Vector Laboratories) was used to stain nuclei and Alexa Fluors (1:500, Invitrogen) were used as secondary antibodies.

To visualize *zen* transcript, fluorescence *in-situ* hybridization was used as described elsewhere[29]. Embryos were hybridized with DIG-labeled antisense probe to *zen* mRNA overnight at 60 °C. Sheep anti-DIG (1:20, Roche) was used as primary antibody and Alexa Fluors (1:500, Invitrogen) were used as secondary antibodies.

Microscopy and gradient quantification

Imaging was performed on a Zeiss LSM510 confocal microscope with a Zeiss 20× (NA 0.6) A-plan objective. High-resolution images (1024 × 1024 pixels, 12 bits depth) were obtained

from the focal plane ~70 μm from either the anterior or posterior pole. For live-imaging, LEICA SP5 confocal microscope was used with 63× (NA 1.3) glycerin objective. Images were obtained every 7 seconds from the focal plane ~70 μm from the anterior pole. We can distinguish anterior and posterior poles by looking for the presence or absence of the pole cells, which are located at the posterior tip of the embryo. Fixed embryos were imaged in 90% glycerol solution and live embryos in PBS buffer.

Protein gradients were extracted from confocal images by using a Matlab program described previously[21]. DAPI staining was used to determine the positions of nuclei, which were then used to quantify the ventral-to-dorsal nuclear concentration gradient of the protein of interest. In order to orient the extracted gradients, the embryos were also co-stained with Dl whose gradient can be used to identify the dorsal-most and ventral-most points of the embryos. Briefly, the extracted nuclear Dl gradient was fitted with a Gaussian curve and the raw data were oriented such that the maximum of the Gaussian fit was set as the ventral-most point of the embryo, i.e. × = 0.

Characterization of flow profile in the micro device by numerical simulation

Simulations were performed using a commercial finite element package, COMSOL®. The three-dimensional geometry of the section of the device is shown in **Supplementary Fig. 1a**. The actual geometry was simplified to contain four actual trap columns to reduce the size of the model and the number of mesh elements. The number of traps in each column in the model (23 total) is the same as that in the actual device. Incompressible steady-state Navier-Stokes equations were solved to obtain the velocity and pressure profiles. The pressure at the outlet was fixed at atmospheric pressure, and the pressure at the inlet was set to obtain a volumetric flow rate equal to the measured value.

Characterization of hydrodynamic force on an embryo by numerical simulation

The simulation described above was used to calculate hydrodynamic force on an embryo located in the trap. The embryo was simplified as described in **Supplementary Fig. 2** at 60° to the trap inlet. The total force in the x-direction were calculated using the post processing feature of COMSOL®, which results in a torque.

Supplementary Material

Refer to Web version on PubMed Central for supplementary material.

ACKNOWLEDGEMENT

The authors acknowledge A. Boettiger and M. Levine (University of California, Berkeley) for the anti-Twist antibody, M. Zhan for technical assistance, A. Boettiger, A. Erives, M. Levine, J. Lippincott-Schwartz, C. Rushlow, M. Serpe, and R. Steward for helpful discussions, and M. Osterfield for assistance with live imaging. This work was supported by National Science Foundation (DBI-0649833 to HL) and National Institutes of Health Grants NS058465 (to HL) and GM078079 (to SYS). HL is a DuPont Young Professor and a Sloan Research Fellow.

References

1. Rushlow CA, Han KY, Manley JL, Levine M. The graded distribution of the Dorsal morphogen is initiated by selective nuclear import transport in Drosophila. Cell. 1989; 59(6):1165–1177. [PubMed: 2598265]
2. Roth S, Stein D, Nusslein-Volhard C. A gradient of nuclear localization of the Dorsal protein determines dorsoventral pattern in the Drosophila embryo. Cell. 1989; 59(6):1189–1202. [PubMed: 2688897]
3. Steward R. Relocalization of the Dorsal protein from the cytoplasm to the nucleus correlates with its function. Cell. 1989; 59(6):1179–1188. [PubMed: 2598266]
4. Luengo Hendriks CL, et al. Three-dimensional morphology and gene expression in the Drosophila blastoderm at cellular resolution I: data acquisition pipeline. Genome Biology. 2006; 7(12)
5. Witzberger MM, Fitzpatrick JAJ, Crowley JC, Minden JS. End-on Imaging: A New Perspective on Dorsoventral Development in Drosophila Embryos. Dev. Dyn. 2008; 237(11):3252–3259. [PubMed: 18855896]
6. Kanodia JS, et al. Dynamics of the Dorsal morphogen gradient. Proc. Natl. Acad. Sci. USA. 2009; 106(51):21707–21712. [PubMed: 19996178]
7. Liberman LM, Reeves GT, Stathopoulos A. Quantitative imaging of the Dorsal nuclear gradient reveals limitations to threshold-dependent patterning in Drosophila. Proc. Natl. Acad. Sci. USA. 2009; 106(52):22317–22322. [PubMed: 20018754]
8. Duffy DC, McDonald JC, Schueller OJA, Whitesides GM. Rapid prototyping of microfluidic systems in poly(dimethylsiloxane). Anal. Chem. 1998; 70(23):4974–4984. [PubMed: 21644679]
9. Quake SR, Scherer A. From micro- to nanofabrication with soft materials. Science. 2000; 290(5496):1536–1540. [PubMed: 11090344]
10. Skelley AM, Kirak O, Suh H, Jaenisch R, Voldman J. Microfluidic control of cell pairing and fusion. Nat. Methods. 2009; 6(2):147–152. [PubMed: 19122668]
11. Tan WH, Takeuchi S. A trap-and-release integrated microfluidic system for dynamic microarray applications. Proc. Natl. Acad. Sci. USA. 2007; 104(4):1146–1151. [PubMed: 17227861]
12. Di Carlo D, Irimia D, Tompkins RG, Toner M. Continuous inertial focusing, ordering, and separation of particles in microchannels. Proc. Natl. Acad. Sci. USA. 2007; 104(48):18892–18897. [PubMed: 18025477]
13. Gervais T, El-Ali J, Gunther A, Jensen KF. Flow-induced deformation of shallow microfluidic channels. Lab on a Chip. 2006; 6(4):500–507. [PubMed: 16572212]
14. Stein D, Roth S, Vogelsang E, Nüsslein-Volhard C. The polarity of the dorsoventral axis in the Drosophila embryo is defined by an extracellular signal. Cell. 1991; 65(5):725–735. [PubMed: 1904007]
15. Govind S, Steward R. Gene regulation: coming to grips with cactus. Curr. Biol. 1993; 3(6):351–354. [PubMed: 15335728]
16. Bothma JP, Levine M, Boettiger A. Morphogen gradients: limits to signaling or limits to measurement? Curr. Biol. 2010; 20(5):R232–234. [PubMed: 20219171]
17. Zinzen RP, Senger K, Levine M, Papatsenko D. Computational models for neurogenic gene expression in the Drosophila embryo. Curr. Biol. 2006; 16(13):1358–1365. [PubMed: 16750631]
18. Belu M, et al. Upright Imaging of Drosophila Embryos. J Vis Exp. 2010; 43:2175. [PubMed: 20864929]
19. Doyle HJ, Kraut R, Levine M. Spatial regulation of zerknüllt: a dorsal-ventral patterning gene in Drosophila. Genes Dev. 1989; 3(10):1518–1533. [PubMed: 2612903]
20. Rushlow C, Colosimo PF, Lin MC, Xu M, Kirov N. Transcriptional regulation of the Drosophila gene zen by competing Smad and Brinker inputs. Genes Dev. 2001; 15(3):340–351. [PubMed: 11159914]
21. Coppey M, Boettiger AN, Berezhkovskii AM, Shvartsman SY. Nuclear Trapping Shapes the Terminal Gradient in the Drosophila Embryo. Curr. Bio. 2008; 18(12):915–919. [PubMed: 18571412]

22. Hong JW, Hendrix DA, Papatsenko D, Levine MS. How the Dorsal gradient works: Insights from postgenome technologies. Proc. Natl. Acad. Sci. USA. 2008; 105(51):20072–20076. [PubMed: 19104040]

23. Mizutani CM, et al. Formation of the BMP activity gradient in the Drosophila embryo. Dev. Cell. 2005; 8(6):915–924. [PubMed: 15935780]

24. Astigarraga S, et al. A MAPK docking site is critical for downregulation of Capicua by Torso and EGFR RTK signaling. EMBO J. 2007; 26(3):668–677. [PubMed: 17255944]

25. Manu, et al. Canalization of Gene Expression in the Drosophila Blastoderm by Gap Gene Cross Regulation. PLoS Biol. 2009; 7(3):591–603.

26. Jaeger J. Modelling the Drosophila embryo. Molecular Biosystems. 2009; 5(12):1549–1568. [PubMed: 20023719]

27. Sanchez L, van Helden J, D. T. Establishement of the dorso-ventral pattern during embryonic development of drosophila melanogasater: a logical analysis. J. Theor. Biol. 1997; 189(4):377–389. [PubMed: 9446747]

28. Umulis DM, Shimmi O, O'Connor MB, Othmer HG. Organism-Scale Modeling of Early Drosophila Patterning via Bone Morphogenetic Proteins. Dev. Cell. 2010; 18(2):260–274. [PubMed: 20159596]

29. Kosman D, et al. Multiplex Detection of RNA Expression in Drosophila Embryos. Science. 2004; 305(5685):846. [PubMed: 15297669]

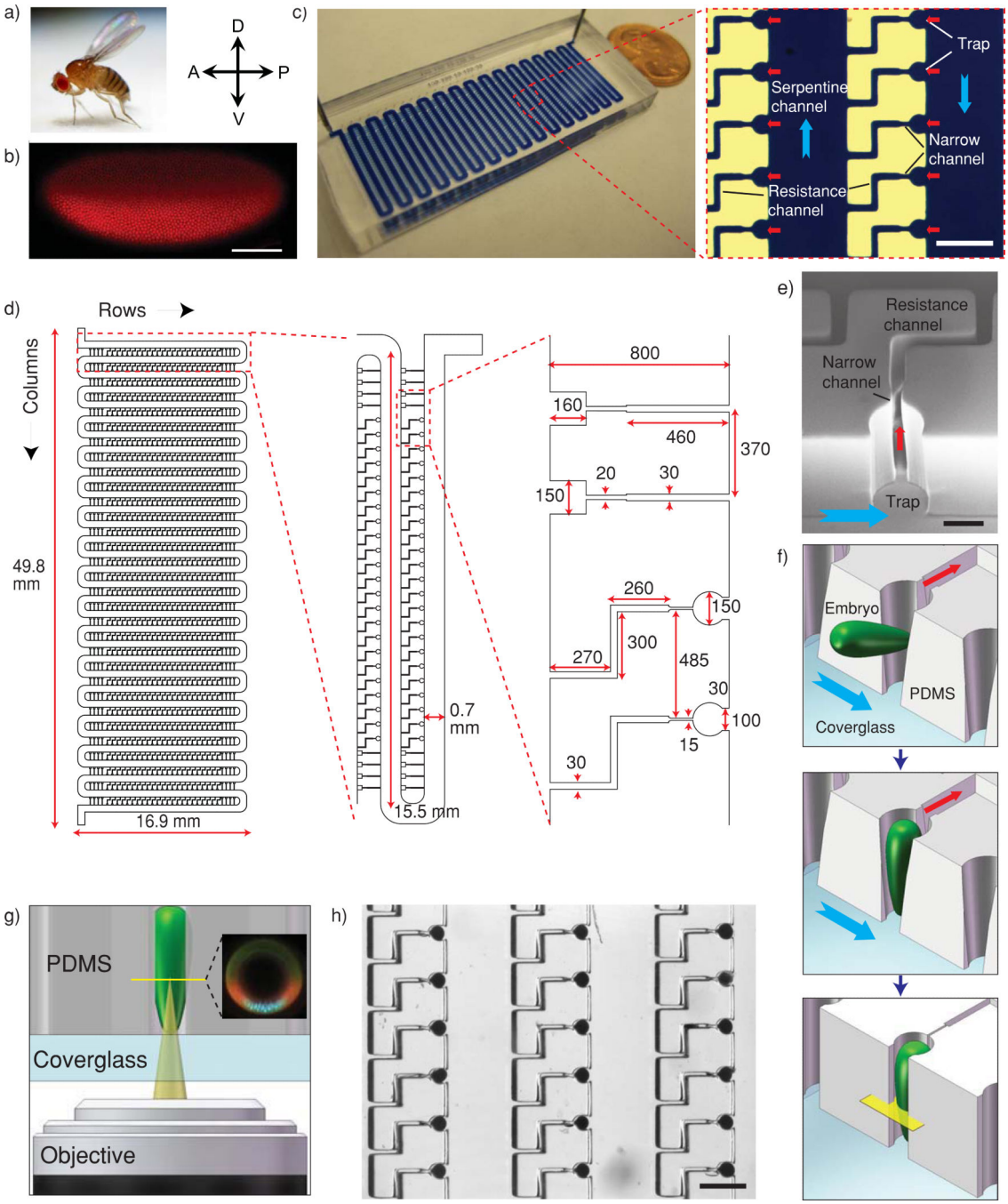

Figure 1.

Microfluidic embryo trap array for high-throughput arraying of vertically-oriented *Drosophila* embryos. The dorsoventral (DV) polarity of the adult *Drosophila* (**a**) is specified in the early embryo (**b**), visualized using anti-Dorsal antibody staining. Image orientation is shown. Scale bar, 100 μm. (**c**) Left, photograph of the device; right, micrograph of the boxed region. Scale bar, 500 μm. (**d**) Details of the embryo trap array design (top view). Numbers have units of μm unless otherwise stated. (**e**) Scanning electron micrograph of the trap structure. Scale bar, 100 μm. (**f**) Schematic showing the embryo trapping process: top, an

embryo is guided into the trap; middle, the flow around the embryo orients it vertically; bottom, the trap contracts secures the embryo. The yellow plane represents imaging focal plane. (**g**) Schematic showing the imaging setup. Inset: representative confocal image of an embryo stained with Dorsal, Twist, and phosphorylated ERK/MAPK. (**h**) The image shows a section of the array with trapped embryos (dark circular object in each trap). Scale bar, 500 μm.

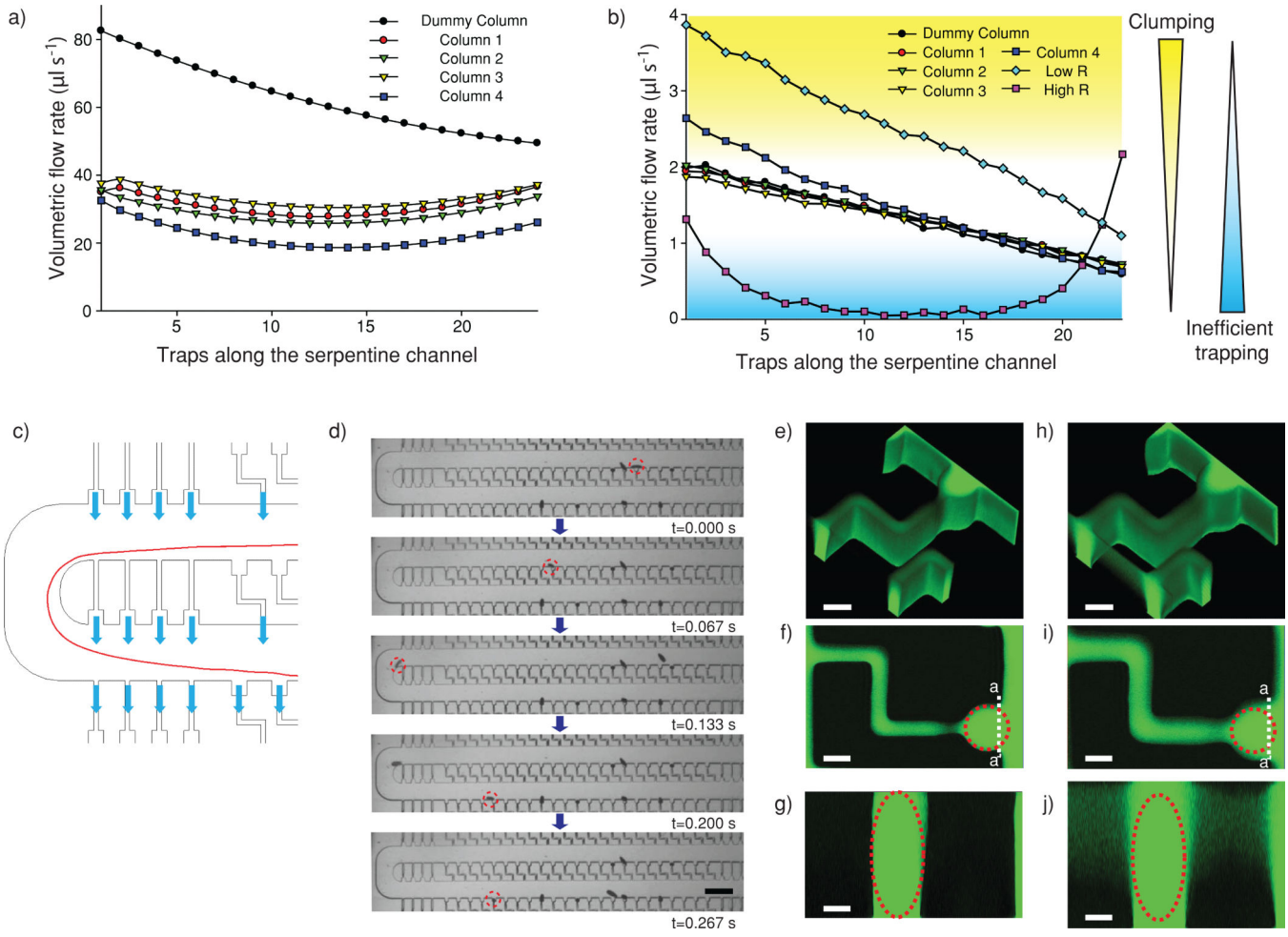

Figure 2.

Operating principles of the embryo trap array. Details of the numerical model are described in the **on-line methods** and **Supplementary Fig. 1**. For (**a-c**), dummy columns are the first and last columns of the device. (a, b) Volumetric flow rate in the serpentine main channel (a) and through the cross-flow channels (b) at each trap. Widths of the resistance channels in the optimal design, low resistance design (Low R), and high resistance design (High R) are 40, 80, and 20 µm respectively. (**c-d**) Dean flow and the converging and diverging flows along the cross-flow channels focus the embryos towards the traps. (**c**) Streamlines plotted from the numerical computational fluid dynamic model (**Supplementary Fig. 1**) as the fluid turns the corner in the main channel. (**d**) Optical images at the indicated time points showing an embryo (red circle) migrating along the wall of the serpentine channel. Scale bar, 800 µm. (**e-j**) Three-dimensional (3D) characterization of the trap by confocal microscopy at 0 psi (**e-g**) and 6 psi (**h-j**). (**f, i**) Single frame top view from the middle of the device. Dotted red circle represents DV plane of an embryo. (**g, j**) Single frame cross-sectional view of the trap opening. Dotted red ellipse represents vertically oriented embryo. Scale bars, 100 µm.

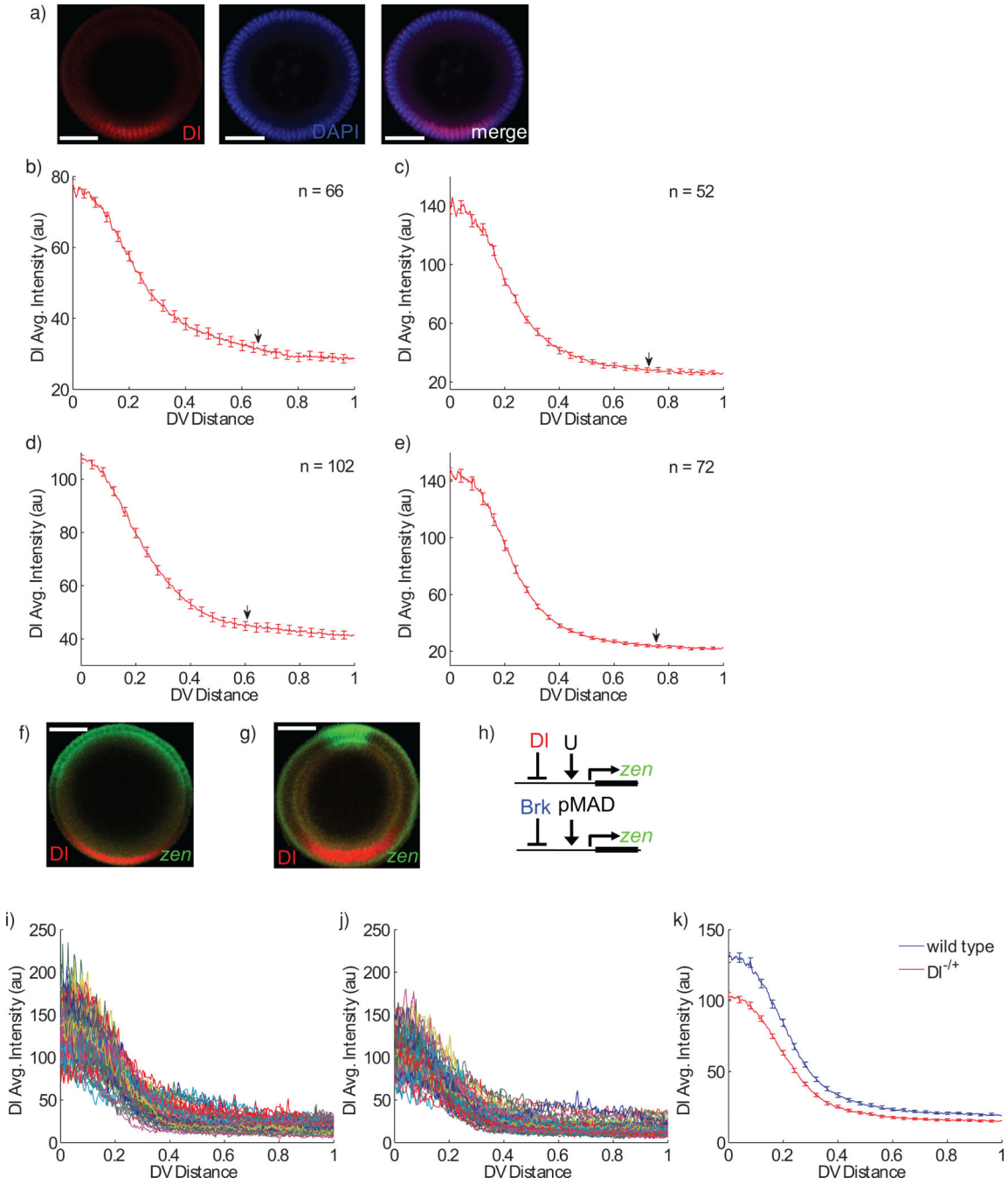

Figure 3.

Spatial extent of the Dl gradient. (**a**) Images show immunofluorescent stain of Dorsal (Dl) and DAPI stain in a vertically oriented embryo. (**b-e**) Average gradients of nuclear Dl from four representative experiments. Error bars are SEM, and the number of gradients used for each experiment is indicated in each plot. The arrow denotes the DV position beyond which the nuclear Dl gradient can be considered flat. (**f-g**) Early (**f**) and late (**g**) expression patterns of Dl and *zen*. (**h**) Schematic of regulatory models that can be used to account for the two phases of *zen* expression (top schematic depicts early expression). (**i-k**) Pair-wise

comparison of Dl gradients in the wild type and mutant backgrounds. (**i, j**) Nuclear Dl gradients from the wild type embryos (**i**) and embryos from *dl* heterozygous females (**j**). (**k**) Average gradients for both genetic backgrounds; error bar are SEM, $n_{WT} = 70$ and $n_{mutant} = 82$.

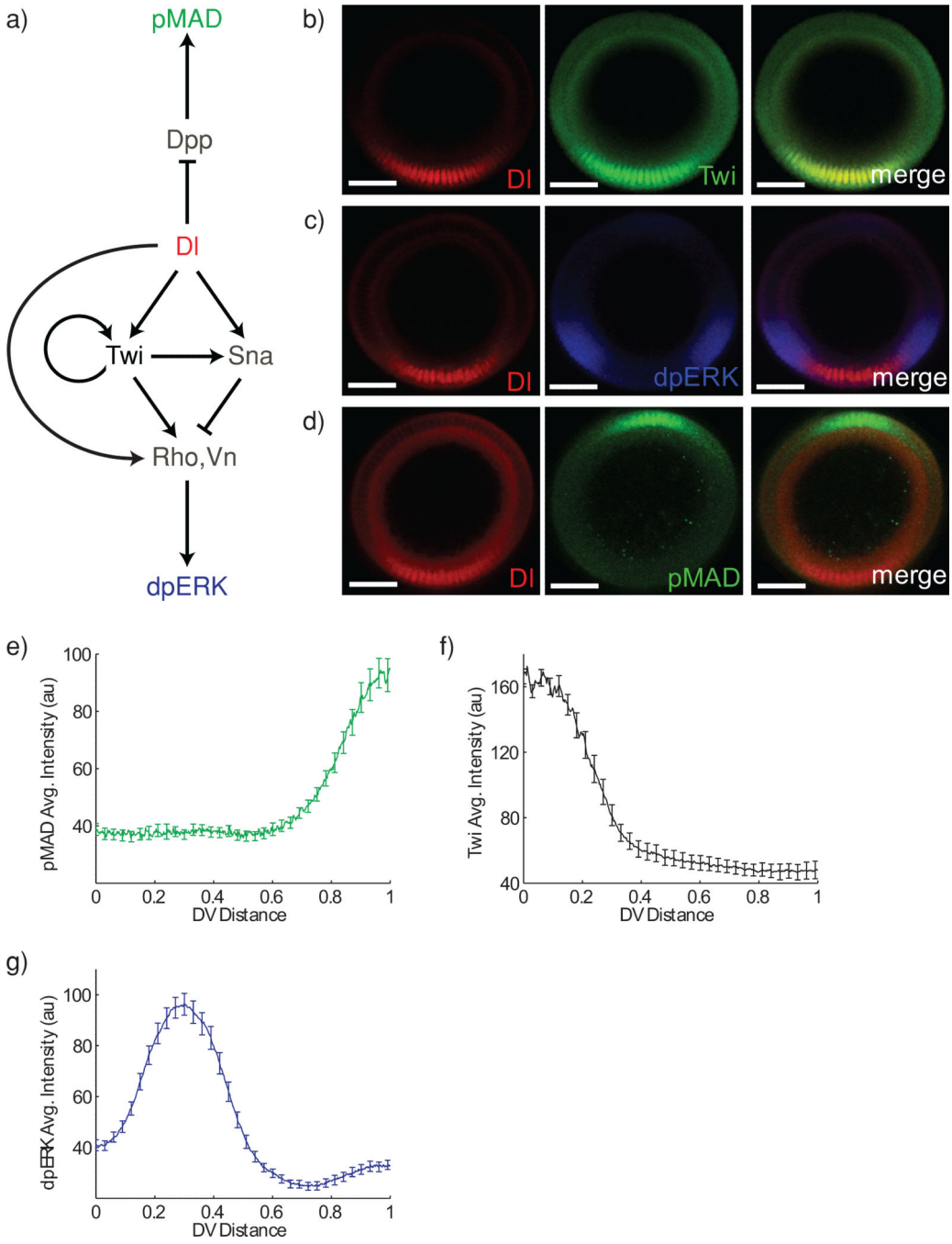

Figure 4.

Quantitative characterization of signal transduction and morphogen gradients in DV patterning. (**a**) A schematic of the DV patterning network, showing the feedforward loops activated by Dl. (**b-d**) Confocal images of embryos immunostained for Dl and Twist (Twi) (**b**), Dl and phospho-MAPK (dpERK) (**c**), and Dl and phospho-MAD (pMAD) (**d**). Scale bar, 25 μm. (**e-g**) Averaged gradients of pMAD (**e**), Twi (**g**), and dpERK (**g**) are plotted; error bars, SEM (n = 64, 40, and 38 gradients, respectively).

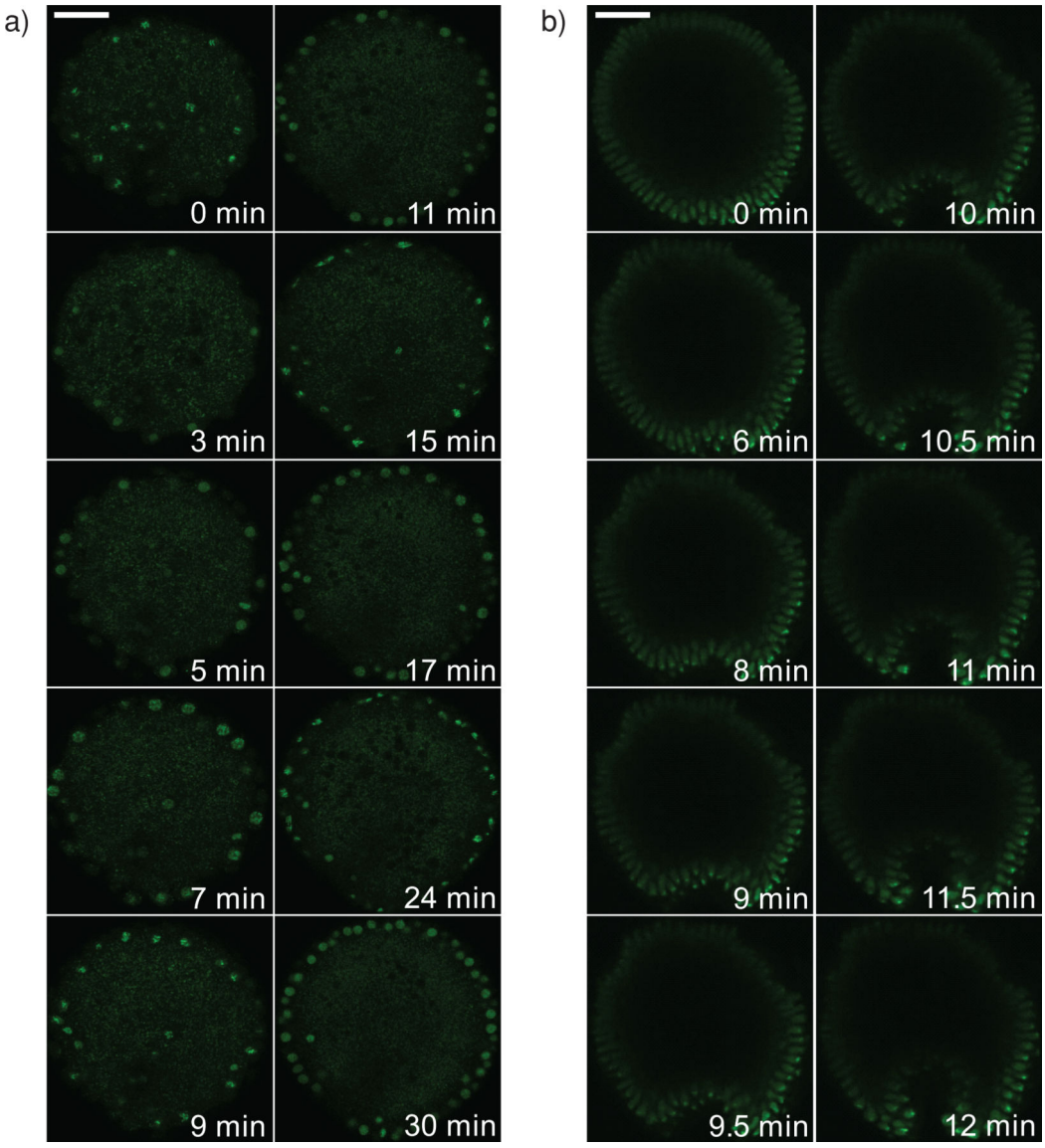

Figure 5.

Live imaging of embryos using the embryo array. (**a, b**) Frames of embryos expressing nuclear histone-GFP undergoing nuclear divisions (a) or ventral invagination (**b**). For both videos, images were taken 70 μm from the anterior pole. (Also see **Supplementary Videos 3 and 4**.) Scale bar, 25 μm.